

Dipole Polarizability of Finite Nuclei as a Probe of Neutron Stars

P.S. Koliogiannis^{1,2}^{*}, E. Yüksel³[†], T. Ghosh¹[‡] and N. Paar¹[§]

¹*Department of Physics, Faculty of Science, University of Zagreb, Bijenička cesta 32, 10000 Zagreb, Croatia*

²*Department of Theoretical Physics, Aristotle University of Thessaloniki, 54124 Thessaloniki, Greece*

³*School of Mathematics and Physics, University of Surrey, Guildford, Surrey, GU2 7XH, United Kingdom*

Nuclear ground state and collective excitation properties provide a means to probe the nuclear matter equation of state and establish connections between observables in finite nuclei and neutron stars. Specifically, the electric dipole polarizability, measured with high precision in various neutron-rich nuclei, serves as a robust constraint on the density dependence of the symmetry energy. In this Letter, we employ a class of relativistic energy density functionals in a twofold process: first, to link the electric dipole polarizability from recent experiments to the slope of the symmetry energy, and second, to translate this information into constraints on the tidal deformability and radii of neutron stars, in connection with multimessenger astrophysical observations from pulsars and binary neutron stars. We provide compelling evidence that the electric dipole polarizability represents a key nuclear observable to probe the neutron star properties. By significantly reducing the uncertainties in the mass-radius plane, our findings also align with recent multimessenger observations.

The equation of state (EoS) of neutron-rich matter governs the structure and properties of neutron stars, shaping key macroscopic characteristics such as mass, radius, and tidal deformability [1–3]. Beyond its astrophysical significance, the EoS is directly linked to nuclear structure through the density dependence of the symmetry energy [4]. In particular, the slope of the symmetry energy L at saturation density ρ_0 plays a crucial role by determining the stiffness of the EoS, which, in turn, influences the neutron star’s internal composition and mass-radius relation, as well as the dynamics of neutron star mergers [2, 5]. Understanding the behavior of the EoS across density scales requires an interdisciplinary approach, combining nuclear physics, gravitational-wave astronomy, high-energy astrophysics, and multimessenger observations [6–18].

Experimental data on finite nuclei provide valuable constraints on the nuclear EoS. For instance, the neutron skin thickness has been shown to directly correlate with the L parameter [2, 5, 19–23]. Notably, Refs. [5, 23] highlight the strong connection between neutron skin thickness in neutron-rich nuclei and neutron star properties, reinforcing the role of nuclear structure experiments in constraining the EoS at supra-nuclear densities. However, precise determination of the neutron skin thickness remains challenging even in the most recent studies using parity-violating electron scattering on ^{48}Ca (CREX) [24] and ^{208}Pb (PREX-2) [25] due to significant experimental uncertainties in measuring neutron radii in nuclei. In addition, CREX and PREX-2 data indicate tension with global energy density functional (EDF) theories [26], yielding inconsistent results for the symmetry energy parameters and neutron skin thickness [27]. Specifically, CREX indicates lower values for these quantities and a *soft* EoS, while PREX-2 results lead to significantly larger values and a *stiff* EoS, both deviating from predictions of other studies [4, 27, 28]. In a recent analysis, new EDFs were calibrated to accommodate constraints from both CREX and PREX-2; however, this calibration shows differences from *ab initio* models and appears to conflict with the NICER observation due to the stiffening of the EoS at high densities relevant to neutron stars [29].

Alternatively, the nuclear electric dipole polarizability α_D ,

which encodes the response of a nucleus to an external electric field, has emerged as a powerful probe of the symmetry energy [30]. The dipole polarizability imposes stringent constraints on the slope of the symmetry energy and, consequently, on the isovector properties of finite nuclei, such as neutron skin thickness [4, 30, 31]. Recent high-precision experiments on neutron-rich nuclei provide dipole polarizability in ^{48}Ca [32], ^{68}Ni [33], $^{112,114,116,118,120,124}\text{Sn}$ [34, 35], and ^{208}Pb [36]. These experimental results have been used to establish a link between dipole polarizability measurements and the symmetry energy in the EDFs, improving the EoS of neutron-rich matter [9, 28, 31, 37–39].

Complementary to available constraints from nuclear experiments, which are mainly effective at low densities, astrophysical observations provide essential insights into the high-density regime of the EoS [2]. Key findings arise from measurements of neutron star masses, which can be precisely determined [40–44], while radius remains significantly more challenging, even with the latest and more accurate constraints from NICER [45–49]. Recent analyses [50–52] have also provided valuable information for the mass-radius plane. The most stringent constraint on neutron star radii comes from the binary neutron star merger GW170817 [53], where the gravitational-wave signal provided direct information on the tidal deformability of the merging stars, leading to improved radius estimates. The tidal deformability enables probing of the symmetry energy at $\sim 2\rho_0$, which can be extrapolated toward saturation density using experimental data from finite nuclei [5]. In this way, a direct connection between astrophysical and nuclear observables can be achieved.

In this Letter, we introduce novel constraints on the neutron star EoS and its associated properties, based on recent experimental data on dipole polarizability in finite nuclei. We employ the relativistic density functional theory incorporating the density-dependent point-coupling (DD-PC) interactions [54, 55], which provides a self-consistent description of both finite nuclei and neutron stars. Specifically, a family of β -equilibrated EoSs is considered, in which the symmetry energy at saturation density is systematically varied from $J = 29$

to 36 MeV, with its corresponding slope ranging from $L = 29$ to 94.1 MeV, thereby covering a wide range [56, 57]. As a first step, we establish a direct connection between experimentally measured values of α_D across various nuclei and the slope parameter L . Then, by using the averaged value of L , we link α_D to astrophysical observables, such as the dimensionless tidal deformability $\Lambda_{1.4}$ and neutron star radius $R_{1.4}$ at $1.4 M_\odot$, thereby establishing a bridge between experiments on finite nuclei and neutron star structure.

To quantify these constraints, we analyze the symmetry energy and its density dependence. The symmetry energy $S_2(\rho)$ can be expanded around the saturation density ρ_0 as $S_2(\rho) = J + Lu + \mathcal{O}(u^2)$, where $u = (\rho - \rho_0)/(3\rho_0)$, and the parameters J and L represent the symmetry energy and its slope at saturation density, respectively (for more details, see Ref. [4]). Furthermore, the electric dipole polarizability, which serves as a key observable for constraining the symmetry energy parameters, is defined through the inverse energy-weighted sum of the dipole response, primarily governed by the properties of isovector giant dipole resonance (IVGDR), a collective oscillation mode of neutrons against protons [4]. It is obtained by integrating the inverse energy-weighted dipole strength function $R(\omega; E1)$ over the excitation energy ω ,

$$\alpha_D = \frac{8\pi e^2}{9} \int_0^\infty \omega^{-1} R(\omega; E1) d\omega, \quad (1)$$

where the $E1$ strength function is calculated using the relativistic quasiparticle random phase approximation (QRPA) [58], adopted for the point-coupling interactions. Similarly, in an astrophysical context, tidal deformability characterizes the response of a neutron star to tidal forces exerted by a companion. It is calculated following the procedure described in Ref. [57].

As an illustrative example, we first consider ^{208}Pb , a benchmark nucleus due to its doubly magic nature and substantial neutron excess. These properties make ^{208}Pb an ideal reference nucleus for studying isovector properties in nuclear models. Figure 1 presents predictions from the DD-PC family of EoSs for the dimensionless tidal deformability of a $1.4 M_\odot$ neutron star, $\Lambda_{1.4}$, as a function of both the electric dipole polarizability α_D and the corresponding neutron star radius $R_{1.4}$. The signal from GW170817 [53], which imposes an upper limit on the neutron star radius, $R_{1.4} = 13.366$ km [57], does not exclude any EoS from the DD-PC family due to the large uncertainty of the observation data. Since all considered EoSs satisfy this limit, the dipole polarizability constraint provides the most stringent bounds on both $\Lambda_{1.4}$ and $R_{1.4}$, as shown in Fig. 1. Specifically, the dipole polarizability of ^{208}Pb yields refined ranges of $313.36 \leq \Lambda_{1.4} \leq 368.47$, $11.96 \leq R_{1.4} \leq 12.15$ km, and a corresponding symmetry energy slope of $39.12 \leq L \leq 55.93$ MeV.

While a neutron-rich nucleus like ^{208}Pb is highly relevant to neutron star matter, a comprehensive analysis, incorporating available experimental data on dipole polarizability across multiple neutron-rich nuclei, is expected to provide more consistent and stringent constraints on L , $\Lambda_{1.4}$, and $R_{1.4}$. In addition, analyzing multiple nuclei tests the robustness of this approach and

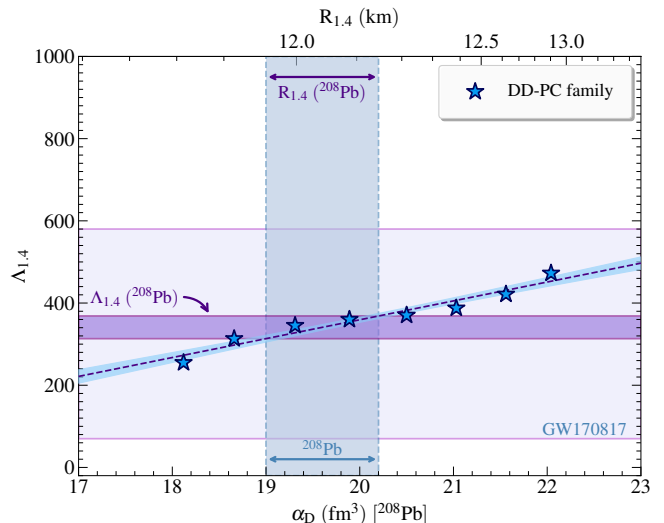


FIG. 1. The dimensionless tidal deformability of a $1.4 M_\odot$ neutron star $\Lambda_{1.4}$ as a function of the electric dipole polarizability α_D of ^{208}Pb and the corresponding neutron star radius for DD-PC EoSs. The horizontal shaded regions mark the limits derived from GW170817 event [53] and those obtained in the present study, while the vertical band denotes the experimental result for α_D [^{208}Pb] and the corresponding neutron star radius inferred in this work.

further refines the density dependence of the symmetry energy. Figure 2 illustrates the relationship between the calculated dipole polarizability and the slope of the symmetry energy for the family of DD-PC interactions. The results are presented for various neutron-rich nuclei with complete experimental data on α_D , including ^{48}Ca , ^{68}Ni , $^{112,114,116,118,120,124}\text{Sn}$, and ^{208}Pb [32–36].

The consistent trends exhibited by DD-PC interactions across these nuclei, combined with their experimental dipole polarizability values, impose a set of independent constraints on the slope of the symmetry energy. To estimate L from the measured α_D , two cases are considered: (a) a subset of four nuclei, denoted as CNSP-4 (^{48}Ca [32], ^{68}Ni [33], ^{120}Sn [34], ^{208}Pb [36]), and (b) the full set of ten nuclei, denoted as CNSP-10, supplementing the CNSP-4 nuclei with more recent measurements of even-even isotopes $^{112-124}\text{Sn}$ [35]. The analysis is performed separately for the two cases because more recent measurements of dipole polarizability in Sn isotopes suggest that a relatively low symmetry energy is needed to reproduce the experimental data [35]. In fact, two recent measurements of ^{120}Sn [34, 35] yield significantly different values of α_D . Through a direct comparison of these data, we conclude that this discrepancy originates from differences in the treatment of excitations above ~ 20 MeV. In Ref. [35] these excitations are described by quasiparticle phonon model, while Ref. [34] incorporates measured data from Ref. [59]. It is important to note that in the high-energy region above 30 MeV, the experimental dipole strength may contain a non-negligible amount of contamination from nonresonant processes, known as the quasideuteron effect [28]. Therefore, for a direct comparison

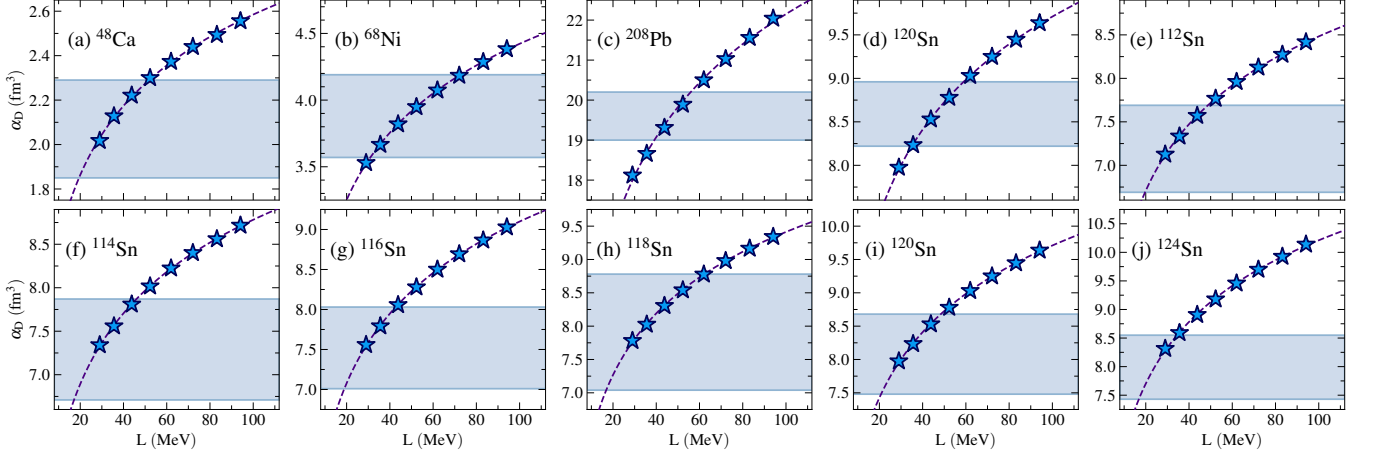


FIG. 2. The electric dipole polarizability α_D as a function of the slope of the symmetry energy L for the DD-PC family of interactions and various isotopes. The horizontal shaded regions represent experimental values on α_D : (a) ^{48}Ca [32], (b) ^{68}Ni [33], (c) ^{208}Pb [28, 36], (d) ^{120}Sn [28, 34], and (e-j) $^{112-124}\text{Sn}$ [35].

with theoretical (Q)RPA calculations, these contributions must be removed, as was done for ^{120}Sn and ^{208}Pb in Ref. [28].

In this work, we determine the weighted average of the slope of the symmetry energy for the two sets of nuclei: $L = 46.08 \pm 6.06$ MeV (CNSP-4) and $L = 37.16 \pm 3.96$ MeV (CNSP-10). Using the same procedure, we also obtain the weighted average of the symmetry energy at saturation density: $J = 31.34 \pm 0.79$ MeV (CNSP-4) and $J = 30.37 \pm 0.64$ MeV (CNSP-10). By incorporating data from multiple nuclei, this approach reduces uncertainties and enhances the reliability of the inferred constraints on the density dependence of the symmetry energy.

Figure 3 shows the dimensionless tidal deformability of a $1.4M_\odot$ neutron star as a function of the slope of the symmetry energy, calculated using the EoSs from the DD-PC family of interactions. The bands corresponding to L values constrained by dipole polarizability data, CNSP-4 and CNSP-10, are also shown. Since the CNSP-4 case leads to slightly stiffer EoSs compared to CNSP-10 ($\Delta L \sim 10$ MeV), the resulting $\Lambda_{1.4}$ values are also higher. Moreover, because the dimensionless tidal deformability scales with the neutron star radius in a power-law relation [57], a similar trend is observed for the radius, which also increases with $\Lambda_{1.4}$. This dependence is depicted in Fig. 3, where the right axis represents the corresponding neutron star radius. Specifically, for the two cases, the following ranges are obtained:

$$\text{CNSP-4:} \quad \begin{cases} 313.80 \leq \Lambda_{1.4} \leq 343.18, \\ 11.92 \leq R_{1.4} \leq 12.12 \text{ km}, \end{cases}$$

$$\text{CNSP-10:} \quad \begin{cases} 298.39 \leq \Lambda_{1.4} \leq 316.35, \\ 11.81 \leq R_{1.4} \leq 11.94 \text{ km}. \end{cases}$$

In addition, the same figure also denotes neutron star radii derived from neutron star merger analyses (vertical arrows) [60, 61], along with the largest (^{118}Sn) and smallest (^{208}Pb) deviations of the L value (horizontal arrows) for reference. It

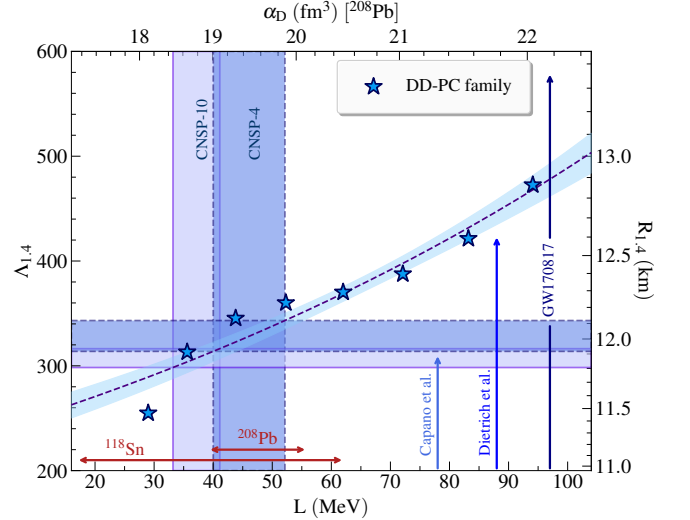


FIG. 3. The dimensionless tidal deformability of a $1.4 M_\odot$ neutron star $\Lambda_{1.4}$ (left axis) and its corresponding radius $R_{1.4}$ (right axis) as a function of the slope of the symmetry energy L for DD-PC EoSs. The dipole polarizability of ^{208}Pb is also shown on the top axis for reference. The vertical shaded regions represent the L values obtained from dipole polarizability for the CNSP-4 and CNSP-10 sets of nuclei, while the horizontal shaded regions denote the corresponding constraints for the $\Lambda_{1.4}$ (or $R_{1.4}$), respectively. Vertical arrows indicate neutron star radii from Refs. [60, 61], and $\Lambda_{1.4}$ from the GW170817 event [53]. Horizontal arrows mark nuclei with the largest and smallest deviations of L value.

should be noted that the constraints for L , $\Lambda_{1.4}$, and $R_{1.4}$ overlap in a rather narrow region, with CNSP-4 yielding higher values than CNSP-10. This outcome is a direct consequence of the inclusion of the dipole polarizability for Sn isotopes from Ref. [35] in the CNSP-10 set of nuclei. In that study, as previously discussed, measurements of α_D result in low values, and, in turn, in lower L values. Since the α_D values for even-even

isotopes $^{112-124}\text{Sn}$ reported in Ref. [35] are not solely based on measured data but also include the higher-energy part of dipole transition strength above 20 MeV calculated within the quasiparticle phonon model, we consider our CNSP-4 results as more reliable for the neutron star properties. Clearly, further and more complete experimental studies are required to provide more consistent and model-independent results for dipole polarizability in Sn isotopes.

Both CNSP-4 and CNSP-10 indicate that the EoS is relatively *soft* in the vicinity of saturation density, consistent with the small neutron star radii inferred from gravitational wave signals of binary neutron star mergers [53]. This agreement between constraints from nuclear experiments and astrophysical observations suggests that the EoS remains soft up to densities corresponding to $1.4 M_{\odot}$ ($\sim 3\rho_0$), with no clear indication of a phase transition within this range. If a transition to exotic degrees of freedom were to occur at lower densities, a more pronounced softening would be expected, potentially conflicting with observed neutron star properties.

We conclude our analysis with Fig. 4, which presents the neutron star gravitational mass as a function of radius for the EoSs of DD-PC functionals, depicted by the extended shaded region. This final figure consolidates constraints from various multimessenger observations, including HESS J1731-347 [50], NICER observations of PSR J1213-1411 [51], PSR J0030+0451 [45, 46], PSR J0437-4715 [52], and PSR J0740+6620 [43, 49], the GW170817 event [53], as well as maximum neutron star masses inferred from pulsar observations [40–44]. Incorporating the more reliable data set for dipole polarizability CNSP-4 refines the DD-PC EoS predictions, narrowing the extended mass-radius region to the inner shaded area. Clearly, the consideration of dipole polarizability significantly reduces uncertainties in the neutron star radius while ensuring consistency with the predicted range [5, 57, 62–64]. Notably, this inner region not only aligns with nuclear experimental constraints but also remains consistent with all considered astrophysical observations, including those from NICER. This highlights the strong agreement between nuclear physics constraints and astrophysical observations, underscoring the robustness of the current neutron star models.

The presented results demonstrate that dipole polarizability serves as a valuable constraint on neutron star properties through the slope of the symmetry energy, a key quantity governing the nuclear matter EoS. Dipole polarizability in nuclei emerges as a promising alternative to the neutron skin thickness, which faces large uncertainties and inconsistent results from recent parity-violating electron scattering experiments [24, 25]. Advancing our understanding of dipole polarizability will significantly improve predictions of neutron star properties and reduce uncertainties in theoretical models. Future measurements of dipole polarizability across various neutron-rich nuclei will be particularly important, as averaging the slope of the symmetry energy from independent experiments will further reduce uncertainties in related neutron star properties. As highlighted in this study, expanding experimental investigations of dipole transitions beyond the

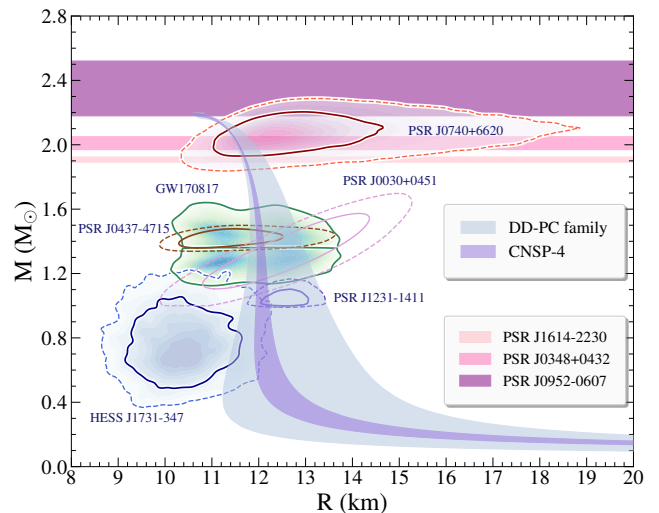


FIG. 4. Gravitational mass as a function of the radius for the DD-PC EoSs, denoted by the extended shaded region. The inner shaded region corresponds to the limits from the CNSP-4 set of nuclei. The shaded contours represent multiple observations, including HESS J1731-347 [50], PSR J1213-1411 [51], PSR J0030+0451 [45, 46], PSR J0437-4715 [52], the GW170817 event [53], and PSR J0740+6620 [43, 49], as well as maximum neutron star masses inferred from pulsar observations [40, 41, 44].

current limit of ~ 20 MeV, especially for even-even isotopes $^{112-124}\text{Sn}$ [35], is essential, given their sizable contribution to the total dipole polarizability.

In addition, the signal from the binary neutron star merger GW170817 has provided significant insights into the nature of dense nuclear matter. Combined with NICER pulsar observations constraining the mass and radius of neutron stars, these multimessenger observations have imposed key constraints on the nuclear matter EoS. As such observations remain our primary window into the properties of dense matter, the forthcoming Einstein Telescope, with its enhanced sensitivity in the lower frequency band, in collaboration with LIGO, Virgo, and KAGRA, is expected to further advance our understanding by detecting fainter signals and extending the reach of neutron star observations.

We are indebted to P. von Neumann-Cosel, A. Tamii, and I. Frišćić for useful discussions which helped to improve various aspects of this study. This work is supported by the Croatian Science Foundation under the project number HRZZ-MOBDOL-12-2023-6026 and under the project Relativistic Nuclear Many-Body Theory in the Multimessenger Observation Era (HRZZ-IP-2022-10-7773). E.Y. acknowledges support from the UK STFC under award no. ST/Y000358/1.

* pkoliogi@phy.hr

† e.yuksel@surrey.ac.uk

‡ tghosh@phy.hr

§ npaar@phy.hr

- [1] J. M. Lattimer and M. Prakash, The physics of neutron stars, *Sci.* **304**, 536 (2004).
- [2] J. Lattimer, Neutron Stars and the Nuclear Matter Equation of State, *Ann. Rev. Nucl. Part. Sci.* **71**, 433 (2021).
- [3] G. Burgio, H.-J. Schulze, I. Vidaña, and J.-B. Wei, Neutron stars and the nuclear equation of state, *Prog. Part. Nucl. Phys.* **120**, 103879 (2021).
- [4] X. Roca-Maza and N. Paar, Nuclear equation of state from ground and collective excited state properties of nuclei, *Prog. Part. Nucl. Phys.* **101**, 96 (2018).
- [5] F. J. Fattoyev, J. Piekarewicz, and C. J. Horowitz, Neutron Skins and Neutron Stars in the Multimessenger Era, *Phys. Rev. Lett.* **120**, 172702 (2018).
- [6] A. W. Steiner, J. M. Lattimer, and E. F. Brown, The Equation of State From Observed Masses and Radii of Neutron Stars, *Astrophys. J.* **722**, 33 (2010).
- [7] S. Goriely, N. Chamel, and J. M. Pearson, Further explorations of Skyrme-Hartree-Fock-Bogoliubov mass formulas. XII. Stiffness and stability of neutron-star matter, *Phys. Rev. C* **82**, 035804 (2010).
- [8] N. Paar, C. C. Moustakidis, T. Marketin, D. Vretenar, and G. A. Lalazissis, Neutron star structure and collective excitations of finite nuclei, *Phys. Rev. C* **90**, 011304 (2014).
- [9] Z. Zhang and L.-W. Chen, Electric dipole polarizability in ^{208}Pb as a probe of the symmetry energy and neutron matter around $\rho_0/3$, *Phys. Rev. C* **92**, 031301 (2015).
- [10] A. L. Watts *et al.*, Colloquium: Measuring the neutron star equation of state using x-ray timing, *Rev. Mod. Phys.* **88**, 021001 (2016).
- [11] F. Özel and P. Freire, Masses, Radii, and the Equation of State of Neutron Stars, *Ann. Rev. Astron. Astrophys.* **54**, 401 (2016).
- [12] M. Oertel, M. Hempel, T. Klähn, and S. Typel, Equations of state for supernovae and compact stars, *Rev. Mod. Phys.* **89**, 015007 (2017).
- [13] B. P. Abbott *et al.* (The LIGO Scientific Collaboration and the Virgo Collaboration), GW170817: Measurements of neutron star radii and equation of state, *Phys. Rev. Lett.* **121**, 161101 (2018).
- [14] H. Tan, J. Noronha-Hostler, and N. Yunes, Neutron Star Equation of State in Light of GW190814, *Phys. Rev. Lett.* **125**, 261104 (2020).
- [15] P. S. Koliogiannis, A. Kanakis-Pegios, and C. C. Moustakidis, Neutron Stars and Gravitational Waves: The Key Role of Nuclear Equation of State, *Foundations* **1**, 217 (2021).
- [16] N. K. Patra, A. Venneti, S. M. A. Imam, A. Mukherjee, and B. K. Agrawal, Systematic analysis of the impacts of symmetry energy parameters on neutron star properties, *Phys. Rev. C* **107**, 055804 (2023).
- [17] S. M. A. Imam, T. Malik, C. m. c. Providência, and B. K. Agrawal, Implications of comprehensive nuclear and astrophysics data on the equations of state of neutron star matter, *Phys. Rev. D* **109**, 103025 (2024).
- [18] C. Y. Tsang, M. B. Tsang, W. G. Lynch, R. Kumar, and C. J. Horowitz, Determination of the equation of state from nuclear experiments and neutron star observations, *Nat. Astron.* **8**, 328 (2024).
- [19] B. Alex Brown, Neutron Radii in Nuclei and the Neutron Equation of State, *Phys. Rev. Lett.* **85**, 5296 (2000).
- [20] S. Typel and B. A. Brown, Neutron radii and the neutron equation of state in relativistic models, *Phys. Rev. C* **64**, 027302 (2001).
- [21] M. Centelles, X. Roca-Maza, X. Viñas, and M. Warda, Nuclear Symmetry Energy Probed by Neutron Skin Thickness of Nuclei, *Phys. Rev. Lett.* **102**, 122502 (2009).
- [22] A. Carbone, G. Colò, A. Bracco, L.-G. Cao, P. F. Bortignon, F. Camera, and O. Wieland, Constraints on the symmetry energy and neutron skins from pygmy resonances in ^{68}Ni and ^{132}Sn , *Phys. Rev. C* **81**, 041301 (2010).
- [23] B. T. Reed, F. J. Fattoyev, C. J. Horowitz, and J. Piekarewicz, Implications of PREX-2 on the Equation of State of Neutron-Rich Matter, *Phys. Rev. Lett.* **126**, 172503 (2021).
- [24] Adhikari *et al.* (CREX Collaboration), Precision Determination of the Neutral Weak Form Factor of ^{48}Ca , *Phys. Rev. Lett.* **129**, 042501 (2022).
- [25] Adhikari *et al.* (PREX Collaboration), Accurate Determination of the Neutron Skin Thickness of ^{208}Pb through Parity-Violation in Electron Scattering, *Phys. Rev. Lett.* **126**, 172502 (2021).
- [26] P.-G. Reinhard, X. Roca-Maza, and W. Nazarewicz, Combined theoretical analysis of the parity-violating asymmetry for ^{48}Ca and ^{208}Pb , *Phys. Rev. Lett.* **129**, 232501 (2022).
- [27] E. Yüksel and N. Paar, Implications of parity-violating electron scattering experiments on ^{48}Ca (CREX) and ^{208}Pb (PREX-II) for nuclear energy density functionals, *Phys. Lett. B* **836**, 137622 (2023).
- [28] X. Roca-Maza, X. Viñas, M. Centelles, B. K. Agrawal, G. Colò, N. Paar, J. Piekarewicz, and D. Vretenar, Neutron skin thickness from the measured electric dipole polarizability in ^{68}Ni , ^{120}Sn , and ^{208}Pb , *Phys. Rev. C* **92**, 064304 (2015).
- [29] B. T. Reed, F. J. Fattoyev, C. J. Horowitz, and J. Piekarewicz, Density dependence of the symmetry energy in the post-PREX-CREX era, *Phys. Rev. C* **109**, 035803 (2024).
- [30] P.-G. Reinhard and W. Nazarewicz, Information content of a new observable: The case of the nuclear neutron skin, *Phys. Rev. C* **81**, 051303 (2010).
- [31] J. Piekarewicz, B. K. Agrawal, G. Colò, W. Nazarewicz, N. Paar, P.-G. Reinhard, X. Roca-Maza, and D. Vretenar, Electric dipole polarizability and the neutron skin, *Phys. Rev. C* **85**, 041302 (2012).
- [32] J. Birkhan *et al.*, Electric Dipole Polarizability of ^{48}Ca and Implications for the Neutron Skin, *Phys. Rev. Lett.* **118**, 252501 (2017).
- [33] D. M. Rossi *et al.*, Measurement of the Dipole Polarizability of the Unstable Neutron-Rich Nucleus ^{68}Ni , *Phys. Rev. Lett.* **111**, 242503 (2013).
- [34] T. Hashimoto *et al.*, Dipole polarizability of ^{120}Sn and nuclear energy density functionals, *Phys. Rev. C* **92**, 031305 (2015).
- [35] S. Bassauer *et al.*, Evolution of the dipole polarizability in the stable tin isotope chain, *Phys. Lett. B* **810**, 135804 (2020).
- [36] A. Tamii *et al.*, Complete Electric Dipole Response and the Neutron Skin in ^{208}Pb , *Phys. Rev. Lett.* **107**, 062502 (2011).
- [37] X. Roca-Maza, M. Brenna, G. Colò, M. Centelles, X. Viñas, B. K. Agrawal, N. Paar, D. Vretenar, and J. Piekarewicz, Electric dipole polarizability in ^{208}Pb : Insights from the droplet model, *Phys. Rev. C* **88**, 024316 (2013).
- [38] Z. Zhang and L.-W. Chen, Constraining the density slope of nuclear symmetry energy at subsaturation densities using electric dipole polarizability in ^{208}Pb , *Phys. Rev. C* **90**, 064317 (2014).
- [39] E. Yüksel, T. Marketin, and N. Paar, Optimizing the relativistic energy density functional with nuclear ground state and collective excitation properties, *Phys. Rev. C* **99**, 034318 (2019).
- [40] Z. Arzoumanian *et al.*, The NANOGrav 11-year Data Set: High-precision Timing of 45 Millisecond Pulsars, *Astrophys. J. Suppl. S.* **235**, 37 (2018).
- [41] J. Antoniadis *et al.*, A Massive Pulsar in a Compact Relativistic Binary, *Sci.* **340**, 1233232 (2013).
- [42] H. Cromartie *et al.*, Relativistic Shapiro delay measurements

- of an extremely massive millisecond pulsar., *Nat. Astron.* **4**, 72 (2020).
- [43] E. Fonseca *et al.*, Refined Mass and Geometric Measurements of the High-mass PSR J0740+6620, *Astrophys. J. Lett.* **915**, L12 (2021).
- [44] R. W. Romani, D. Kandel, A. V. Filippenko, T. G. Brink, and W. Zheng, PSR J0952-0607: The Fastest and Heaviest Known Galactic Neutron Star, *Astrophys. J. Lett.* **934**, L17 (2022).
- [45] M. C. Miller *et al.*, PSR J0030+0451 Mass and Radius from NICER Data and Implications for the Properties of Neutron Star Matter, *Astrophys. J. Lett.* **887**, L24 (2019).
- [46] T. E. Riley *et al.*, A NICER View of PSR J0030+0451: Millisecond Pulsar Parameter Estimation, *Astrophys. J. Lett.* **887**, L21 (2019).
- [47] M. C. Miller *et al.*, The Radius of PSR J0740+6620 from NICER and XMM-Newton Data, *Astrophys. J. Lett.* **918**, L28 (2021).
- [48] T. E. Riley *et al.*, A NICER View of the Massive Pulsar PSR J0740+6620 Informed by Radio Timing and XMM-Newton Spectroscopy, *Astrophys. J. Lett.* **918**, L27 (2021).
- [49] A. J. Dittmann *et al.*, A More Precise Measurement of the Radius of PSR J0740+6620 Using Updated NICER Data, *Astrophys. J.* **974**, 295 (2024).
- [50] V. Doroshenko, V. Suleimanov, G. Pühlhofer, and A. Santangelo, A strangely light neutron star within a supernova remnant., *Nat. Astron.* **6**, 1444–1451 (2022).
- [51] T. Salmi *et al.*, A NICER View of PSR J1231-1411: A Complex Case, *Astrophys. J.* **976**, 58 (2024).
- [52] D. Choudhury *et al.*, A NICER View of the Nearest and Brightest Millisecond Pulsar: PSR J0437–4715, *Astrophys. J. Lett.* **971**, L20 (2024).
- [53] B. P. Abbott *et al.* (LIGO Scientific Collaboration and Virgo Collaboration), Properties of the Binary Neutron Star Merger GW170817, *Phys. Rev. X* **9**, 011001 (2019).
- [54] T. Nikšić, D. Vretenar, and P. Ring, Relativistic nuclear energy density functionals: Adjusting parameters to binding energies, *Phys. Rev. C* **78**, 034318 (2008).
- [55] T. Nikšić, N. Paar, D. Vretenar, and P. Ring, DIRHB—A relativistic self-consistent mean-field framework for atomic nuclei, *Comp. Phys. Comm.* **185**, 1808 (2014).
- [56] E. Yüksel, T. Oishi, and N. Paar, Nuclear Equation of State in the Relativistic Point-Coupling Model Constrained by Excitations in Finite Nuclei, *Universe* **7**, 71 (2021).
- [57] P. Koliogiannis, E. Yüksel, and N. Paar, Constraining neutron star properties through parity-violating electron scattering experiments and relativistic point coupling interactions, *Phys. Lett. B* **862**, 139362 (2025).
- [58] N. Paar, P. Ring, T. Nikšić, and D. Vretenar, Quasiparticle random phase approximation based on the relativistic Hartree-Bogoliubov model, *Phys. Rev. C* **67**, 034312 (2003).
- [59] S. C. Fultz, B. L. Berman, J. T. Caldwell, R. L. Bramblett, and M. A. Kelly, Photoneutron Cross Sections for Sn^{116} , Sn^{117} , Sn^{118} , Sn^{119} , Sn^{120} , Sn^{124} , and Indium, *Phys. Rev.* **186**, 1255 (1969).
- [60] C. D. Capano, I. Tews, S. M. Brown, B. Margalit, S. De, S. Kumar, D. A. Brown, B. Krishnan, and S. Reddy, Stringent constraints on neutron-star radii from multimessenger observations and nuclear theory, *Nat. Astron.* **4**, 625 (2020).
- [61] T. Dietrich, M. W. Coughlin, P. T. H. Pang, M. Bulla, J. Heinzel, L. Issa, I. Tews, and S. Antier, Multimessenger constraints on the neutron-star equation of state and the Hubble constant, *Sci.* **370**, 1450 (2020).
- [62] C. Tsang, M. Tsang, P. Danielewicz, F. Fattoyev, and W. Lynch, Insights on Skyrme parameters from GW170817, *Phys. Lett. B* **796**, 1 (2019).
- [63] T. Malik, N. Alam, M. Fortin, C. Providência, B. K. Agrawal, T. K. Jha, B. Kumar, and S. K. Patra, GW170817: Constraining the nuclear matter equation of state from the neutron star tidal deformability, *Phys. Rev. C* **98**, 035804 (2018).
- [64] E. Annala, T. Gorda, A. Kurkela, and A. Vuorinen, Gravitational-Wave Constraints on the Neutron-Star-Matter Equation of State, *Phys. Rev. Lett.* **120**, 172703 (2018).